Title: Propagating ice front induces gas bursts and ultrasonic acoustic emissions from freezing xylem

Authors: Anna Lintunen[1,2], Adriano Losso[3], Juho Aalto[1], Tommy Chan[1], Teemu Hölttä[2], and Stefan Mayr[3]

Contact info:

[1]Institute for Atmospheric and Earth System Research / Physics, Faculty of Science, P.O. Box 64, FI-00014 University of Helsinki, Finland

[2]Institute for Atmospheric and Earth System Research / Forest Sciences, Faculty of Agriculture and Forestry, P.O. Box 27, FI-00014 University of Helsinki, Finland

[3]Department of Botany, University of Innsbruck, Sternwartestrasse 15, A-6020 Innsbruck, Austria

Correspondence: Anna Lintunen

Email: anna.lintunen@helsinki.fi

Running title: Freezing-induced gas bursts and acoustic emissions

Keywords: acoustic emissions; bark permeability; freeze–thaw cycles; effective diffusion coefficient of CO_2; respiration; winter embolism

Abstract

Ice formation and propagation in the xylem of plants is a complex process. During freezing of xylem sap, gases dissolved in liquid sap are forced out of the ice lattice due to their low solubility in ice, and supersaturation of xylem sap as well as low water potential (Ψ) are induced at the ice–liquid interface. Supersaturation of gases near the ice front may lead to bubble formation and potentially to cavitation and/or to burst of gases driven out from the branch. In this study, we investigated the origin and dynamics of freezing-related gas bursts and ultrasonic acoustic emissions (AEs), which are suggested to indicate cavitation. *Picea abies* and *Salix caprea* branch segments were exposed to frost cycles in a temperature test chamber, and CO_2 efflux (indicating gas bursts) and AEs were recorded. On freezing, two-thirds of the observed gas bursts originated from the xylem and only one third from the bark. Simultaneously with gas bursts, AEs were detected. Branch Ψ affected both gas bursts and AEs, with high gas burst in saturated and dry samples but relevant AEs only in the latter. Repeated frost cycles led to decreasing gas burst volumes and AE activity. Experiments revealed that the expanding ice front in freezing xylem was responsible for observed gas bursts and AEs, and that branch Ψ influenced both processes. Results also indicated that gas bursts and cavitation are independently induced by ice formation, though both may be relevant for bubble dynamics during freezing.

1. Introduction

Ice formation in wood is a complex dynamic process. At subzero temperatures, xylem sap can be in a doubly metastable state, when it is under tension and supercooled (Caupin et al. 2015). While increasing tension may induce cavitation, decreasing temperatures will lead to ice nucleation, after which ice will propagate longitudinally and radially within the xylem (Neuner et al. 2010, Pramsohler et al. 2012, Charrier et al. 2017). Freezing can damage plants at the cellular level by plasmolysis or intracellular ice formation, which is lethal for cells (Ristic & Ashworth 1993, Pearce 2001, Ruelland et al. 2009, Charrier et al. 2013). Furthermore, frost cycles can cause embolism and, as a consequence, loss of xylem hydraulic conductivity (Tyree & Sperry 1989, Sperry & Sullivan 1992, Tyree et al. 1994, Mayr et al. 2007, Charrier et al. 2014). Following the classical theory of freeze-thaw-induced embolism, embolism occurs because gases, dissolved in unfrozen xylem sap, are hardly soluble in ice. During freezing, gases segregate and form bubbles within the ice (Sucoff 1969, Sperry & Sullivan 1992, Mayr & Sperry 2010, Sevanto et al. 2012, Charra-Vaskou et al. 2015). Upon thawing, these bubbles collapse and gases dissolve back into the sap. However, in the case of large bubbles and/or tension in the surrounding xylem sap, the bubbles can expand, fill the conduit, and lead to embolism (Pittermann & Sperry 2006, Mayr & Améglio 2016).

A visualization of bubble formation in freezing xylem sap has not yet been possible, but several studies reported ultrasonic acoustic emissions (AEs) to occur during ice formation (Raschi et al. 1989, Kikuta & Richter 2003, Mayr et al. 2007, Mayr & Zublasing 2010, Charrier et al. 2015). Under drought, AEs enable the detection of cavitation, i.e. the rapid tension release in the conduits when liquid water at low water potential (Ψ) is replaced by water vapor near vacuum pressure (Tyree & Dixon 1983, Salleo & Lo Gullo 1986, Mayr & Rosner 2011, Charrier

et al. 2015). During freezing, the mechanism producing AEs is less clear, but previous studies indicated that AEs during freezing are caused by cavitation in the xylem sap due to low Ψ at the ice–liquid interface (Mayr et al. 2007, Mayr & Sperry 2010, Charrier et al. 2015, 2017). This suggests that there might be two embolism mechanisms involved in embolism formation of tree stems during frost cycles: the freeze-thaw-induced embolism (according to classical theory; Sucoff 1969, Sperry & Sullivan 1992, Mayr & Sperry 2010, Sevanto et al. 2012, Charra-Vaskou et al. 2015) and freeze-induced cavitation at the propagating ice front (producing AEs; Mayr et al. 2007, Mayr & Sperry 2010, Charrier et al. 2015, 2017).

It was also shown that freezing can lead to emission of gases from xylem tissues—Lintunen et al. (2014) demonstrated for the first time, that gases were pushed out from conifer stems during ice propagation both in laboratory experiments and under field conditions. These results suggest that a proportion of gases dissolved in the xylem sap can be emitted from the xylem during freezing and is not trapped in ice. However, it is still unknown, from which tissue(s) the observed gas bursts originate and the underlying processes are not yet understood. It is likely that gas concentrations in front of the propagating ice front increase (Sevanto et al. 2012) and thus create a large concentration gradient between gases inside conduits and inter-conduit spaces (as well as ambient air). This gradient may accelerate the diffusion of gases out from the stem until the entire sap is frozen. In addition to this diffusion process, gases may be driven out from the vascular system by pressure-driven mass flow (Lintunen et al. 2014). The volume increase upon water–ice transition creates positive pressure (Robson & Petty 1987), which will force gases to escape from the conduits much faster than by diffusion only. Theoretical calculations of gas volumes (Lintunen et al. 2014) suggest that bursts might reduce the likelihood of embolism formation during the freezing process by decreasing the sap gas content.

In this study, we monitored the spatial and dynamic patterns of gas bursts and AEs of branches to analyze the effects of branch water status and the role of xylem and bark. Also, we studied potential links between gas bursts and AEs. Branch segments of *Picea abies* were exposed to frost cycles in a temperature test chamber, and gas bursts and AEs of saturated and dehydrated stems and peeled xylem as well as detached bark samples were measured. Measurements were also performed during repeated frost cycles, and additional freeze–thaw experiments on a broad-leaved species (*Salix caprea*). We hypothesized that (i) gas bursts (measured as CO_2 efflux) originating from the xylem are larger than from the bark as proposed based on theoretical calculations by Lintunen et al. (2014); (ii) gas bursts and AEs occur simultaneously; and (iii) the volume of gas bursts and the number of AEs depend on branch Ψ, with the highest gas bursts and AEs recorded in medium dry samples. In fact, we expect freezing-induced cavitation to be absent in saturated samples, while in completely dehydrated samples, the remaining volume of the xylem sap should be too small for relevant gas bursts or AEs. Finally, (iv) repeated frost cycles were expected to cause a decrease in gas bursts and AEs as embolism formation would reduce the probability of cavitation and gas bursts would reduce sap gas concentrations in consecutive frost cycles. Based on this first simultaneous analyses of gas efflux (measured as CO_2 efflux) and AEs, the identification of stem tissues producing the gas burst and the analysis of the influence of water potentials, this study should enable new insights into the complex process of freezing in plant xylem.

2. Material and methods

2.1. Plant material

Picea abies (L.) H. Karst. branches (1 to 1.5 m long) were collected from mature trees growing at Natters (47°11′N, 11°12′E, 838 m a.s.l.) near the Institute of Botany in Innsbruck, Austria. Sixteen branches were collected during the first week of March 2018 and the first 2 weeks of April 2018, before the start of the vegetation period. In addition, three branches of *Salix caprea* L. were collected during the second week of April at the alpine timberline (Praxmar, Tyrolean Central Alps, Austria; 47°09′N, 11°07′E; 1680 m a.s.l.). *P. abies* and *S. caprea* species were selected as they are typical temperate/boreal species growing in extreme habitats, and thus are exposed to numerous frost cycles during winter.

Immediately after collection, branches were covered with black plastic bags and saturated in a bucket filled with tap water for at least 24 h. After saturation, Ψ was measured from 2–4 end twigs (ca 10 cm) per branch with a pressure chamber (PMS, model 1505D, Albany, NY, USA). A 10 cm long segment was cut under water from the base of each branch, and the remaining 35 cm long branch segment, without side branches, was further used for experiments (later referred to as sample). After cutting, the ends of the sample were immediately sealed with instant adhesive (Loctite 382 Instant Adhesive, Henkel, Düsseldorf, Germany) to minimize drying of the sample during the experiment.

2.2. Ultrasonic acoustic emissions

Ultrasonic AE measurements were performed with a PCI-8-based system (PAC Micro-II Express Digital AE System) and 150 kHz resonance sensors (R15) connected to a preamplifier set to 40 dB (Physical Acoustics, Wolfegg, Germany). The threshold was set to 45 dB and the gain to 40 dB (Mayr et al. 2007, Mayr & Rosner 2011, Charrier et al. 2015). With these settings, AEs can be detected over several centimeters in conifers. Registration and analysis of AEs were

147 performed with AEwin software (Mistras Holdings Corp., Princeton, NJ, USA). Ultrasonic
148 sensors were attached to both ends of the samples (Fig. 1). On stem samples, a small square (1
149 × 1 cm) of the bark was removed to attach the sensors, and silicone grease was used to allow
150 good contact between the sensors and the xylem surface.
151
152 2.3. Gas exchange measurements
153
154 A cuvette (outside length 10 cm; inside length 5.5 cm; diameter varied with branch size and
155 mounting) made of transparent polyethylene plastic was wrapped around the central part of the
156 sample, sealed at both ends with foam, and tightened with cable ties (Fig. 1). The joint of the
157 cuvette was sealed with transparent tape. To allow constant air circulation, gas inlet and outlet
158 tubes were connected to the cuvette and a battery-powered fan (1 lpm) was inserted into the
159 cuvette (Fig. 1).
160
161 The gas exchange of the sample was measured with a mobile CO_2 and H_2O open-flow cuvette
162 system that includes a high-resolution LI-840A gas analyzer (LI-COR, Lincoln, NE, USA). A
163 Raspberry Pi computer was used to communicate with the gas analyzer, via an 8-channel
164 transmitter (Nokeval, Nokia, Finland) and user-defined measuring protocols. The system was
165 powered by a 48 Ah lead acid battery (Optima Batteries, WI, USA) and the measurement
166 system was dynamic, such that it allowed supply air from a single source (ambient or cylinder
167 air) to enter two cuvettes and a reference line (Fig. 2). Supply air was continuously passed
168 through the cuvettes at a constant rate, and measurements were based on the concentration of
169 the air stream flowing out of the cuvette and reference airline. The system was designed to
170 measure three air samples in the following alternating order: air sample from the first cuvette,
171 air sample from the reference line (that fed substitute air for compensating the flush and sample

flows from the cuvettes), and air sample from the second cuvette. The flows through the cuvettes and reference lines were controlled via valves, which were turned on and off following a measurement cycle. The flow rates for measurements and flushing during the supply air measurement were set to 0.56 lpm.

2.4. Freezing experiments

To study CO_2 bursts and AEs during freezing, we conducted freezing experiments in a temperature test chamber (Binder model MK 53, Tuttlingen, Germany). Gas exchange cuvettes and AE sensors were first installed onto samples. Further, two T-type thermocouples were positioned in the xylem located inside the cuvette with 2 cm distance from each other, and two thermocouples were positioned in the xylem located outside the cuvette (on both ends of the branch segment; see Fig. 1). Thermocouples allowed constant detection of xylem temperature and thus enabled to record when the xylem sap froze. Freezing releases thermal energy due to the phase change from water into ice (Burke et al. 1976) and, therefore, it is possible to detect sudden increases in local xylem temperature (i.e. freezing exotherm), which indicate freezing xylem sap. Xylem temperatures were measured at 10 s intervals and logged with a data logger (Campbell Scientific, Logan, UT, USA).

Samples were exposed to a temperature cycle inside the test chamber. The temperature was first set to +2°C for 45 min before cooling for a period of 1 h to reach a temperature of −8°C. Then, the temperature was kept at −8°C for 1 h before warming for 1 h to reach back +2°C. As last step, the temperature was kept constant at +2°C for a minimum of 30 min (see Supporting Information). As with previous freezing studies, similar freezing/thawing rates were used to reduce the time needed for each experiment (Mayr et al. 2007, Mayr & Sperry 2010, Lintunen

et al. 2014). The temperature inside the gas exchange cuvette was always higher than in the surrounding test chamber but the temperature difference never exceeded +3.5°C. This was enabled by positioning the supply air tubing on the test chamber floor (loops with a total length of ca 2m) to allow heat transfer between the metallic test chamber and the tubing before it reached the cuvette. Drying of the samples during the experiments was expected to be small, because the cut ends of the branches were sealed and temperature of the test chamber decreased to +2°C fast in the beginning of the experiment.

Based on these settings, several freezing experiments were conducted. In experiment 1, we tested for the origins of freezing-related CO_2 bursts (xylem, bark, or both). The bark was carefully detached from three saturated *P. abies* samples as a single piece (i.e., bark samples included the phloem and outer bark). The detached bark was then positioned around a plastic tube and stabilized with small cable ties to prevent excess drying from the inner surface of the bark. Parallel to the detached bark sample, the peeled xylem sample was measured in the second cuvette. In experiment 2, we analyzed the influence of Ψ on the CO_2 bursts and AEs. After saturation, prior to exposure to the temperature cycles, *P. abies* samples were dehydrated to a Ψ between −3.2 MPa and −3.4 MPa (hereafter called "dry"; 3 samples) and to a Ψ below −4 MPa (hereafter called "very dry"; 3 samples). Four branches were kept saturated (Ψ between −0.3 MPa and −0.5 MPa). In experiment 3, we studied the dynamics of CO_2 bursts and AEs during three repeated frost cycles with four saturated *P. abies* samples. In other words, the same cycle (from +2°C to −8°C) was repeated three times, and between cycles the temperature was kept for 1 h at +2°C. In experiment 4, we studied CO_2 bursts in three saturated samples of *S. caprea* L.

Freezing was artificially induced in all samples to decrease the variability of the freezing temperature and to control the point of ice nucleation. The tip of a copper nail, which was previously cooled via liquid nitrogen, was used to touch a 1 × 2 cm debarked section of the branch (see also Fig. 1) at the sample base. Freezing was induced when the xylem temperature at the stem base (outside the cuvette) was around −1.5°C in the saturated samples and around -3.0°C in the dehydrated samples to mimic their natural freezing temperatures (Lintunen et al. 2018). In experiment 3, artificial freezing was induced at the stem base at −1.5°C in the first two cycles, while freezing occurred spontaneously in the third cycle (due to the dehydrated surface of the debarked section, induction of freezing was not possible).

2.5. Calculation of the freezing-related CO_2 burst and effective diffusion coefficient for CO_2

The exchange of CO_2 between the stem and its environment can be directly measured, while it is necessary to exclude respiration effects from the measured CO_2 efflux to calculate the magnitude of the freezing-related CO_2 burst. At above freezing temperatures, stem CO_2 exchange and respiration are tightly coupled to each other, (albeit with a time lag; see Teskey & McGuire 2007, Bloemen et al. 2013), while they are clearly decoupled during and after freezing. Very little information exists on the temperature dependence of the respiration rate in a frozen stems, therefore, we assumed similar temperature dependence before and after freezing (i.e., the temperature dependency of respiration was extrapolated to below freezing temperatures). The magnitude of the freezing-related CO_2 burst is thus affected by CO_2 produced by respiration (i.e., the concentration gradient between the inside and outside of the stem), the effective radial diffusion coefficient for CO_2, and the partial pressure difference between the inside and outside of the stem. We used a previously published dynamic model of CO_2 mass balance and transport within the stem (Hölttä & Kolari 2009, Lintunen et al. 2014)

to separate the freezing-related CO_2 burst from the total stem CO_2 efflux and to estimate the effective radial CO_2 diffusion coefficient for the samples. The model (Hölttä & Kolari 2009) solves the CO_2 concentration profile within the stem by taking into account the CO_2 produced in respiration, its partitioning between the liquid and gaseous phase, and its radial diffusion according to the concentration gradient within the stem. The change in the amount of CO_2 (ΔN_{CO2}, µmol) inside the stem during a time interval Δt (s) can be expressed as:

$$\Delta N_{CO2} / \Delta t = R(T_{xylem}) - (C_{CO2} - C_{CO2,\,amb})\, d_{eff} \quad (1)$$

where d_{eff} ($m^3\ s^{-1}$) is an effective diffusion coefficient (Heitjans & Kärger 2005, including information on size, geometry, and water content of the object, i.e., it is the constant of proportionality between the flux of CO_2 due to diffusion and the difference in the concentration between the inside of the stem and the ambient air) and R respiration rate (µmol s^{-1}), C_{CO2} is the CO_2 concentration in the air phase inside the stem, and $C_{CO2,amb}$ is the ambient CO_2 concentration inside the climate chamber. We modelled R to be exponentially dependent on temperature inside the unfrozen stem ($T_{xylem,}$ °C): A Q10 value of 2.5 was used for the temperature dependency of respiration, similarly to the original parameterization. $R\,(T_{xylem})$ was fitted separately to each experiment based on the measurements before freezing. We assumed both gaseous (see Gartner et al. 2004) and liquid phases to account for 25% of stem volume. The relationship between CO_2 concentration in gaseous and liquid phase was calculated by the Henry's law (Seinfeld & Pandis 1998), which strongly depends on temperature. Model parameterization was kept as described in Lintunen et al. (2014).

The difference between the total measured CO_2 efflux (which includes respired CO_2 and freezing-related CO_2 burst) and the modeled CO_2 efflux (includes only respired CO_2) represents

271 the burst of CO_2 released from the stem due to the freezing process. The volume of the freezing-
272 related CO_2 burst was calculated as an integral of this difference from the moment of ice
273 nucleation until the difference went to zero or the apoplastic water thawed at about 0°C (in
274 some cases the burst was not over when the stem thawed). Values of the radial diffusion
275 coefficient and absolute respiration were both fitted so that the dynamics and absolute values of
276 the modeled CO_2 efflux rate matched the measured CO_2 efflux rate until the stem was frozen.
277
278 We also calculated the volume of freezing-related CO_2 bursts normalized to the respiration rate
279 of the sample at +5°C, (i.e., the volume of the burst was divided by the respiration efflux of the
280 sample at +5°C; hereafter called "normalized CO_2 burst"). In this way, samples with different
281 respiration levels, and thus a different amount of stored CO_2, could be compared.
282
283 2.6. Statistical analysis
284
285 Statistical analysis was performed with the GLM procedure in SAS ver. 9.4 (SAS Institute,
286 Cary, NC, USA), which uses the method of least squares to fit general linear models. Analysis
287 of variance was used to compare the volume of the freezing-related CO_2 bursts, number of AEs,
288 respiration at +5°C, and effective diffusion coefficient of CO_2 between samples of different Ψ,
289 samples with peeled xylem, detached bark or both (i.e. intact branch), and samples of different
290 species. In the analysis comparing samples with different Ψ, data were unbalanced due to
291 different sample sizes between treatments. Therefore, a Type III test was used in GLM, because
292 this test is independent of the number of observations per treatment combination. All tests were
293 performed at a probability level of 5%. Values are given as mean ± standard error.
294
295 **3. Results**

3.1. Freezing-related CO_2 bursts from peeled xylem and detached bark

In experiment 1, freezing-related CO_2 bursts were detected in both peeled xylem samples and detached bark samples of *P. abies* (Fig. 3A, B). In detached bark, the volume of absolute CO_2 bursts was about 3.4-fold lower ($P = 0.043$) and the volume of normalized CO_2 bursts about 7-fold ($P = 0.010$) lower than that of intact samples (Fig. 4A). Neither the volume of absolute nor normalized CO_2 bursts differed between peeled xylem and intact samples (Fig. 4A). CO_2 efflux per surface area at +5°C did not differ between detached bark, peeled xylem or intact samples (not shown). The effective CO_2 diffusion coefficient was higher in detached bark than in peeled xylem or intact samples ($P < 0.001$), whereas there was no significant difference between peeled xylem and intact samples (Fig. 4A).

3.2. CO_2 efflux and acoustic emission dynamics at different water potential

In experiment 2, samples showed decreasing CO_2 efflux with decreasing xylem temperature until freezing occurred (Fig. 5A). The average level of CO_2 efflux at +5°C was 0.52 ± 0.06 µmol m^{-2} s^{-1} and it decreased down to 0.30 ± 0.03 µmol m^{-2} s^{-1} prior to freezing. CO_2 efflux increased in all samples simultaneously with freezing, which was indicated by a freezing exotherm (Fig. 5A). The average maximum CO_2 efflux during the freezing exotherm was 0.42 ± 0.03 µmol m^{-2} s^{-1}. There was no statistical difference between saturated and dehydrated samples in the CO_2 efflux at +5°C or in the freezing-related CO_2 bursts. However, the volume of the freezing-related normalized CO_2 bursts in saturated and dry samples was 3.4-fold and 3.1-fold higher than in very dry samples, respectively (Fig. 6A). In contrast, the effective diffusion coefficient of CO_2 was 6.9-fold and 2.9-fold higher in very dry samples than in

saturated and dry samples, respectively (Fig. 6B, the sample with Ψ of −6.7 MPa was dropped from the analysis as an outlier).

Freezing-related CO_2 bursts were not always completed before thawing. This was particularly obvious in saturated stems, which also showed long-lasting freezing exotherms. However, the CO_2 efflux was always highest soon after the beginning of the exotherm and decreased toward the onset of thawing. Thus, the potential bias in the calculated burst volume is expected to be small.

Besides CO_2 efflux, we also observed AEs during freezing (Fig. 5B). At the stem base (where ice nucleation was induced), the onset of AEs was always registered parallel to the start of the exotherm. AEs ceased when the exotherm peaked, until the temperature decreased again and new AEs were observed. The cumulative number of AEs was highest in samples with a Ψ between −2.5 MPa and −3.5 MPa (Fig. 6C). At the stem apex (AE2 sensor in Fig. 1), the cumulative number of AEs was smaller than at the stem base and sometimes even missing. The onset of AEs was always later at the apex than at the stem base (Fig. 5B).

3.3 CO_2 efflux and acoustic emission dynamics in subsequent frost cycles

During three subsequent frost cycles (experiment 3), CO_2 measurements indicated a pronounced freezing-related CO_2 burst in the first cycle, a smaller one in the second, and a barely visible one in the third (Fig. 7). Unfortunately, the volume of the bursts could not be calculated due to difficulty in modeling respiration-induced CO_2 efflux between the repeated frost cycles. Interestingly, CO_2 efflux was also detected during thawing, whereby these thawing-induced bursts increased with consecutive temperature cycles. AEs, like in experiment

2, were only observed during freezing, whereby the number of cumulative AEs was highest in the first cycle and decreased during consecutive cycles (Fig. 7).

3.4. Comparing CO_2 efflux and acoustic emission dynamics of *Salix caprea*

Freezing-related CO_2 bursts were also detected from saturated samples of *S. caprea* (Fig. 8A; experiment 4). The absolute volume of the bursts was not significantly different between species, but the volume of the normalized CO_2 bursts with respiration rate at +5°C was lower in *S. caprea* than in *P. abies* ($P = 0.021$; Fig. 4B). This can be partly explained by the lower respiration rate of *P. abies* at +5°C compared with that of *S. caprea* ($P < 0.001$) (Fig. 4B). Also, burst dynamics differed between species as the CO_2 bursts started earlier (already at the time of ice nucleation outside the gas exchange cuvette) and were shorter in *S. caprea* than in *P. abies* (Fig. 8). The effective CO_2 diffusion coefficient was clearly higher in *S. caprea* than in *P. abies* ($P = 0.029$; Fig. 4B). The dynamics and patterns of AEs during freezing were similar to *P. abies*, with highest acoustic activity immediately after exotherm detection and a time lag between the two sensors (Fig. 8).

4. Discussion

Performed temperature experiments on *P. abies* demonstrated a high complexity of the freezing process in xylem, with respective complex dynamics and patterns in gas bursts and AEs. Our hypotheses were partly confirmed: (i) the majority of the CO_2 efflux originated from the xylem; (ii) freezing-related gas bursts and AEs occurred simultaneously with freezing, indicating that the propagating ice front induced both; (iii) branch Ψ had a major influence on both gas bursts and AEs, though the gas burst was high in saturated and medium dry samples, while relevant

AEs were only observed in medium dry samples; and (iv) repeated frost cycles led to decreasing gas burst volumes and AE activity. In addition, CO_2 bursts and AEs were demonstrated in *S. caprea*, which indicates that the observed processes are relevant in conifer as well as angiosperm species.

Experiment 1 demonstrated that about two thirds of released CO_2 came from the xylem, while only one third originated from the bark, despite the high proportion of living tissues and large intercellular spaces in the latter. In a previous study on *Pinus sylvestris* and *P. abies* (Lintunen et al. 2014), a modeling approach suggested that the volume of freezing-related CO_2 bursts corresponded to 70% of the total amount of dissolved CO_2 in the xylem. When we now consider that one third of the gas burst originated from the bark, we can conclude that about 50% of the total CO_2 within the xylem is released via a gas burst on freezing. It is important to note that xylem sap also contains other dissolved gases, with N_2 and O_2 representing the highest volumes. Analyzed CO_2 burst dynamics, therefore, should be qualitatively equivalent to bursts of other gases but differ quantitatively due to differences in concentration in xylem sap and the ambient air, solubility and diffusion coefficients. The main source of CO_2 within the bark was most likely within the intercellular spaces, which were filled with ice during freezing. This is because living cells in hardened *P. abies* stems avoid lethal intracellular ice formation by extracellular freezing (Sakai & Okada 1971). The effective radial CO_2 diffusion coefficient at +5°C was clearly higher in the detached bark than in peeled xylem and intact samples, most likely due to the more porous bark tissue. The effective radial diffusion coefficient of CO_2 has only rarely been measured for stems and varied between 10^{-11} m^2 s^{-1} and 10^{-7} m^2 s^{-1}, depending on wood structure and water status (Sorz & Hietz 2006, Spicer & Holbrook 2007, Hölttä & Kolari 2009). Our calculation of 10^{-9} m^2 s^{-1} for *P. abies* stems (Fig. 4) falls well within this range.

396 CO_2 bursts were strongly influenced by the water status of the samples (experiment 2). The
397 volume of normalized CO_2 bursts detected during freezing was lower in dehydrated samples
398 (Fig. 6; very dry) probably due to the following reasons. First, the sap volume (because of
399 drought-induced embolism preceding frost treatment) and respective absolute volume of gases
400 dissolved in the sap was low, and the volumetric increase upon water–ice transition was small.
401 Second, a lower Ψ causes lower freezing temperatures (Lintunen et al. 2018), which leads to
402 higher ice propagation velocities (Kitaura 1967, Langer et al. 1978, Hacker & Neuner 2007,
403 Rauschenberger et al. 2013, Charrier et al. 2015). A low Ψ is thus associated with small CO_2
404 bursts because high ice propagation velocities may not leave enough time for the gases to
405 diffuse out of the stem before being trapped in ice. Third, the effective radial diffusion
406 coefficient of CO_2 at +5°C was negatively related to stem Ψ (Fig. 6). This can be explained by
407 the higher portion of air in dry stems as the diffusion of gases is about 10 000 times faster in air
408 than in water (Nobel, 2005). Diffusion of CO_2 out of dry stems might lead to a low internal CO_2
409 gas concentration prior to freezing and thus to small gas bursts on freezing. In very dry samples,
410 the number of AEs was also small, probably because most conduits were already air-filled due
411 to drought-induced embolism. In contrast, samples between −3.2 MPa and −3.4 MPa (Fig. 6;
412 dry) showed a high number of AEs as well as pronounced gas bursts. Previous studies (Mayr
413 et al. 2007, Mayr & Sperry 2010, Charrier et al. 2015, 2017), indicated that AEs are induced by
414 cavitation events near the moving ice front, causing a sudden release of tension. Mayr et al.
415 (2007) clearly demonstrated that AEs during freezing are related to xylem water under tension
416 as samples at critical water potential showed highest acoustic activity while saturated samples
417 (or water in a straw) did hardly emit AEs. Charrier et al. (2015) found that AEs in freezing
418 samples of several tree species showed two distinct phases: the first phase during ice nucleation
419 and propagation, and the second after dissipation of the exothermal heat. They explained the
420 first phase of AEs by low water potential of ice at the ice–liquid interface, which induced

numerous and strong signals. This in accordance with our experiments, where the sensor near the point of artificial ice nucleation always recorded AEs earlier than the distal sensor (Fig. 3). Remarkably, the comparison of saturated and dry samples demonstrated that cavitation (indicated by AEs) and gas bursts, although both induced by ice formation, are not directly linked: gas bursts from dry samples were likely not solely related to cavitation events as saturated samples (Fig. 6; saturated) showed nearly identical, high CO_2 effluxes.

Both freezing-related CO_2 bursts and AEs were detected during each of the three consecutive frost cycles in experiment 3 (Fig. 7). However, the volume of the bursts and the number of AEs strongly decreased from the first to the third cycle. The number of AEs per freezing event has already been shown to decrease in a study by Mayr et al. (2007). The authors suggested that tracheids, which embolized during the first frost cycle, cannot cavitate a second time and thus the number of cavitating conduits (and respective AEs) decreases during subsequent frost cycles. CO_2 bursts decreased during consecutive frost cycles because there was not probably enough time for the accumulation of new CO_2 from tissue respiration in the xylem between the frost cycles to replace CO_2 lost in the bursts. Also, embolized xylem portions may provide additional diffusion pathways out of the stem, which enable gas effluxes during thawing. Accordingly, CO_2 bursts during thawing (also see Fig. 3) increased on each subsequent frost cycle. Further studies are required to disentangle the complex interrelations of processes during freezing and thawing, Ψ, and repeated frost cycles.

Freezing-induced gas bursts and AEs were also detected in *S. caprea* (Fig. 8), suggesting that simultaneous CO_2 bursts and AEs are a phenomenon which can be found in many species. Interestingly, neither of our study species exhibited an increase in CO_2 efflux before the freezing exotherm was observed. In contrast, Sperling et al. (2015) reported significant

446 increases in stem respiration upon response to near-freezing temperatures in several woody
447 species growing in temperate environments. The authors found that the increase in CO_2 efflux
448 before freezing was related to an acceleration of stem non-structural carbohydrate consumption.
449 We did not observe an effect in CO_2 efflux even when *P. abies* samples were kept near (but
450 above) the freezing point for a longer time (data not shown) and thus it is unlikely that metabolic
451 activity played a role in observed gas bursts. Our experiments also demonstrated that the
452 majority of the CO_2 efflux originated from xylem tissue (which mainly consists of dead conduit
453 cells), and that the bursts occurred simultaneously with and not before ice nucleation. However,
454 freezing-tolerant species growing at high elevation and/or latitudes differ in their temperature-
455 dependent respiration patterns from temperate species, which might lead to interspecific
456 differences in freezing-related CO_2 burst dynamics and patterns.
457
458 **5. Conclusion**
459
460 Potential mechanisms underlying freezing-related patterns observed in the present study are
461 summarized in Fig. 9: ice propagation forces gases out of the freezing sap, so they either form
462 bubbles (which are then trapped in ice) or move away from the ice front and remain dissolved
463 in the sap. In the latter case, the gas concentration in the remaining sap increases (Sevanto et al.
464 2012), thus increasing the driving force for gases to escape from the conduit via diffusion
465 (leading to freezing-related gas burst). The detection of AEs during freezing indicates cavitation
466 events (i.e., bubble formation) near the ice–liquid interface due to high tensions induced by ice
467 (Mayr et al. 2007, Charrier et al. 2015). In this case, cavitation would result in a sudden release
468 of tension inside the conduits and, consequently, in AEs. Accordingly, saturated samples show
469 larger gas bursts as they contain larger gas volumes dissolved in the sap but emit only a few (or
470 no) AEs as the tension in the sap is low (Fig. 9). In dry samples, higher tensions in the xylem

lead to more AEs. Very dry samples contain a higher number of embolized conduits, which contribute neither to gas bursts nor AEs.

Our study clearly indicates that processes occurring near the expanding ice front in freezing xylem are responsible for observed gas burst and AE patterns. However, many aspects of the freezing process in plant xylem (e.g., the small-scale spatial pattern of ice propagation, ice formation through the pits, bubble formation) as well as the influence of environmental factors (e.g., temperature gradients within xylem, growth conditions) and the relevance for plant life exposed to freezing require further study.

Conflict of interest

The authors confirm that there are no conflicts of interest to declare.

Funding

This work was supported by the Academy of Finland (grants number 310375, 307331).

Acknowledgements

We thank technician Heikki Laakso for building the gas exchange measurement system used in this study, and technician Birgit Dämon for her technical help in the laboratory.

Author contributions

A. Lintunen, S. Mayr, and T. Hölttä planned, and A. Lintunen, A. Losso and S. Mayr conducted, the experiments. J. Aalto and T. Chan designed and built the gas measurement system together with technician H. Laakso. T. Hölttä was responsible for the calculation of the freezing-related burst and A. Lintunen for the statistical analysis. A. Lintunen had the main responsibility for writing the paper, but all authors contributed to the writing process.

References

Bloemen J, McGuire MA, Aubrey DP, Teskey RO, Steppe K (2013) Assimilation of xylem-transported CO_2 is dependent on transpiration rate but is small relative to atmospheric fixation. J Exp Bot 64: 2129-2138.

Burke MJ, Gusta LV, Quamme HA, Weiser CJ, Li PH (1976) Freezing and injury in plants. Ann Rev Plant Physiol 27: 507-528.

Caupin F (2015) Escaping the no man's land: Recent experiments on metastable liquid water. Journal of Non-Crystalline Solids 407: 441-448.

Charra-Vaskou K, Badela E, Charrier G, Ponomarenko A, Bonhomme M, Foucat L, Mayr S, Améglio T (2015) Cavitation and water fluxes driven by ice water potential in *Juglans regia* during freeze–thaw cycles. J Exp Bot 67: 739-750.

Charrier G, Charra-Vaskou K, Kasuga J, Cochard H, Mayr S, Améglio T (2014) Freeze–thaw stress: effects of temperature on hydraulic conductivity and ultrasonic activity in ten woody angiosperms. Plant Physiol 164: 992-998.

Charrier G, Nolf M, Leitinger G, Charra-Vaskou K, Losso A, Tappeiner U, Améglio T, Mayr S (2017) Monitoring of freezing dynamics in trees: a simple phase shift causes complexity. Plant Physiol 173: 2196-2207.

527 Charrier G, Poirier M, Bonhomme M, Lacointe A, Améglio T (2013) Frost acclimation in
528 different organs of walnut trees *Juglans regia* L.: how to link physiology and modelling? Tree
529 Physiol 33: 1229-1241.
530
531 Charrier G, Pramsohler M, Charra-Vaskou K, Saudreau M, Améglio T, Neuner G, Mayr S
532 (2015) Ultrasonic emissions during ice nucleation and propagation in plant xylem. New Phytol
533 207: 570-578.
534
535 Gartner BL, Moore JR, Gardiner BA (2004) Gas in stems: abundance and potential
536 consequences for tree biomechanics. Tree Physiol 24: 1239-1250.
537
538 Hacker J, Neuner G (2007) Ice propagation in plants visualized at the tissue level by infrared
539 differential thermal analysis (IDTA). Tree Physiol 27: 1661-1670.
540
541 Heitjans P, Kärger J (2005) Diffusion in Condensed Matter. Heidelberg: Springer.
542
543 Hölttä T, Kolari P (2009) Interpretation of stem CO_2 efflux measurements. Tree Physiol 29:
544 1447-1456.
545
546 Kikuta SB, Richter H (2003) Ultrasound acoustic emissions from freezing xylem. Plant Cell
547 Environ 26: 383-388.
548
549 Kitaura K (1967) Supercooling and ice formation in Mulberry trees. In: Asahina E ed. Cellular
550 injury and resistance in freezing organisms. Proceedings of international conference on low
551 temperature science. Sapporo: Bunyeido Printing Co, 143-156.

552

553 Langer JS, Sekerka RF, Fujioka T (1978) Evidence for a universal law of dendritic growth
554 rates. J Cryst Growth 44: 414-418.

555

556 Lintunen A, Lindfors L, Kolari P, Juurola E, Nikinmaa E, Hölttä T (2014) Bursts of CO_2
557 released during freezing offer a new perspective on avoidance of winter embolism in trees.
558 Ann Bot 114: 1711-1718.

559

560 Lintunen A, Mayr S, Salmon Y, Cochard H, Hölttä T (2018) Drivers of apoplastic freezing in
561 gymnosperm and angiosperm branches. Ecol Evol 8: 333-342.

562

563 Mayr S, Améglio T (2016) Freezing stress in tree xylem. In: Lüttge U, Cánovas F, Matyssek
564 R, eds. Progress in Botany 77. Cham: Springer, 381-414.

565

566 Mayr S, Cochard H, Améglio T, Kikuta SB (2007) Embolism formation during freezing in the
567 wood of *Picea abies*. Plant Physiol 143: 60-67.

568

569 Mayr S, Rosner S (2011) Cavitation in dehydrating xylem of *Picea abies*: energy properties
570 of ultrasonic emissions reflect tracheid dimensions. Tree Physiol 31: 59-67.

571

572 Mayr S, Sperry JS (2010) Freeze–thaw-induced embolism in *Pinus contorta*: centrifuge
573 experiments validate the 'thaw-expansion hypothesis' but conflict with ultrasonic emission
574 data. New Phytol 185: 1016-1024.

575

Mayr S, Zublasing V (2010) Ultrasonic emissions from conifer xylem exposed to repeated freezing. J Plant Physiol 167: 34-40.

Neuner G, Xu B, Hacker J (2010) Velocity and pattern of ice propagation and deep supercooling in woody stems of *Castanea sativa*, *Morus nigra* and *Quercus robur* measured by IDTA. Tree Physiol 30: 1037-1045.

Nobel PS (2005) Physiochemical and environmental plant physiology. New York: WH Freeman and Company.

Pearce RS (2001) Plant freezing and damage. Ann Bot 87: 417-424.

Pittermann J, Sperry JS (2006) Analysis of freeze-thaw embolism in conifers. The interaction between cavitation pressure and tracheid size. Plant Physiol 140: 374-382.

Pramsohler M, Hacker J, Neuner G. 2012. Freezing pattern and frost-killing temperature of apple (*Malus domestica*) wood under controlled conditions and in nature. Tree Physiol 32: 819-828.

Raschi A, Scarascia Mugnozza G, Surace R, Valentini R, Vazzana C (1989) The use of ultrasound technique to monitor freezing and thawing of water in plants. Agr Ecosyst Environ 27: 411-418.

599 Rauschenberger P, Criscione A, Eisenschmidt K, Kintea D, Jarkilić S, Tuković Z, Roisman
600 IV, Weigand B, Tropea C (2013) Comparative assessment of volume-of- fluid and level-set
601 methods by relevance to dendritic ice growth in supercooled water. Comp Fluids 79: 44-52.
602
603 Ristic Z, Ashworth EN (1993) Ultrastructural evidence that intracellular ice formation and
604 possibly cavitation are the sources of freezing injury of supercooling wood tissue of *Cornus*
605 *florida* L. Plant Physiol 103: 753-761.
606
607 Robson DJ, Petty JA (1987) Freezing in conifer xylem I. Pressure changes and growth
608 velocity of ice. J Exp Bot 38: 1901-1908.
609
610 Ruelland E, Vaultier MN, Zachowski A, Hurry V (2009) Cold signaling and cold acclimation
611 in plants. Adv Bot Res 49: 35-150.
612
613 Sakai A, Okada S (1971) Freezing resistance of conifers. Silvae Genetica 20: 91-97.
614
615 Salleo S, Lo Gullo MA (1986) Xylem cavitation in nodes and internodes of whole *Chorisia*
616 *insignis* H. B. et K. plants subjected to water stress. Relations between xylem conduit size and
617 cavitation. Ann Bot 58: 431-441.
618
619 Seinfeld JH, Pandis SN (1998) Atmospheric chemistry and physics: from air pollution to
620 climate change. New York: Wiley & Sons.
621
622 Sevanto S, Holbrook NM, Ball M (2012) Freeze/thaw-induced embolism: probability of
623 critical bubble formation depends on speed of ice formation. Front Plant Sci 3: 107.

624

625 Sorz J, Hietz P (2006) Gas diffusion through wood: implications for oxygen supply. Trees 20:
626 34-41.

627

628 Sperling O, Earles JM, Secchi F, Godfrey J, Zwieniecki MA (2015) Frost induces respiration
629 and accelerates carbon depletion in trees. PLOS ONE, doi:
630 https://doi.org/10.1371/journal.pone.0144124

631

632 Sperry JS, Sullivan JEM (1992) Xylem embolism in response to freeze–thaw cycles and water
633 stress in ring-porous, diffuse-porous and conifer species. Plant Physiol 100: 605-613.

634

635 Spicer R, Holbrook NM (2007) Effects of carbon dioxide and oxygen on sapwood respiration
636 in five temperate tree species. J Exp Bot 58: 1313-1320.

637

638 Sucoff E (1969) Freezing of conifer xylem and the cohesion–tension theory. Physiol
639 Plantarum 22: 424-431.

640

641 Teskey RO, McGuire MA (2007) Measurement of stem respiration of sycamore (*Platanus*
642 *occidentalis* L.) trees involves internal and external fluxes of CO_2 and possible transport of
643 CO_2 from roots. Plant Cell Environ 30: 570-579.

644

645 Tyree MT, Davis SD, Cochard H (1994) Biophysical perspectives of xylem evolution: is there
646 a tradeoff of hydraulic efficiency for vulnerability to dysfunction? IAWA J 15: 335-360.

647

Tyree MT, Dixon MA (1983) Cavitation events in *Thuja occidentalis* L.? Ultrasonic acoustic emissions from the sapwood can be measured. Plant Physiol 72: 1094-1099.

Tyree MT, Sperry JS (1989) Vulnerability of xylem to cavitation and embolism. Annu Rev Plant Physiol Plant Mol Biol 40: 19-38.

Figure legends

Figure 1. Cuvette and measurement setup. Both ends of the branch segment (brown) were sealed with glue (light blue) and a transparent cuvette was wrapped around the central part of the sample. The cuvette was sealed at both ends with foam (black), and gas inlet and outlet tubes (dark blue) were connected to the cuvette. To allow constant air circulation, a battery-powered mini fan (1 lpm) was inserted. The system for measuring gas exchange is presented in Fig. 2. Two acoustic emission (AE) sensors and two thermocouples (T) were attached to both sides of the cuvette—AE1 and T1 at the base and AE2 and T4 at the apex. Two thermocouples were also inserted inside the cuvette—T2 at the base and T3 at the apex. A small square (1 × 2 cm) of the bark was removed at the stem base to enable artificial freezing.

Figure 2. Schematic diagram of the gas exchange measurement system for simultaneous measurements of two samples. Circles with an internal triangle represent the pumps, and S0, S1, S2, F1, and F2 are the valves. MFM refers to Mass Flow Meter. Because of using pressurized air from a cylinder, the pump and buffer for the supply air were bypassed (shown with a dashed line). The measurement consists of a stepwise program that is repeated: i) both cuvettes are first flushed with supply air for 30 s and the supply air concentration is measured during the flushing. ii) The supply air line for cuvette 1 is closed and the concentration in the cuvette is measured for 60s; meanwhile, cuvette 2 continues to be flushed with supply air. iii) Both cuvettes are again flushed with supply air for 30s, and the supply air concentration is measured during the flushing. iv) The supply air line for cuvette 2 is closed and the concentration in the cuvette is measured for 60s; meanwhile, cuvette 1 continues to be flushed with supply air. Figure 1 shows how the cuvette was mounted on the sample.

679 Figure 3. Time series of a measured CO_2 efflux and a modeled respiratory CO_2 release from a
680 peeled *Picea abies* sample (A) and detached bark (B). At the beginning of the experiment, the
681 sample water potential was −1.5 MPa. Xylem temperatures inside the cuvette are shown (T2
682 and T3). The background color represents the frozen (white) and thawed (light gray) periods of
683 the xylem sap.
684
685 Figure 4. A) Comparison of the average volume of freezing-related CO_2 bursts, freezing-related
686 CO_2 bursts normalized with respiration efflux at +5°C, and the effective CO_2 diffusion
687 coefficient for peeled xylem, detached bark, and intact samples (i.e. samples including both
688 xylem and phloem) of saturated *Picea abies*. There was no difference between peeled xylem,
689 detached bark, and intact samples in the respiration efflux at +5°C. B) Comparison of the
690 average volume of freezing-related CO_2 bursts, normalized CO_2 bursts, and respiration efflux
691 at +5°C between saturated samples of *P. abies* and *Salix caprea*. There was no difference
692 between species in the effective CO_2 diffusion coefficient. Significant differences ($P < 0.05$)
693 between groups are indicated by different letters and roman numbers. Mean ± standard error.
694
695 Figure 5. Time series of a measured CO_2 efflux and a modeled respiratory CO_2 release (A) and
696 acoustic emissions (AEs) (B) measured on a *P. abies* sample dehydrated to −3.4 MPa. Xylem
697 temperatures inside the cuvette (T2 and T3) are shown in A, whereas xylem temperatures
698 outside the cuvette (T1 and T4) are shown in B. The background color represents the frozen
699 (white) and thawed (light gray) periods of the xylem sap.
700
701 Figure 6. Comparison of the volume of freezing-related CO_2 bursts normalized with respiration
702 at +5°C (A), effective diffusion coefficient of CO_2 (B), and total number of acoustic emissions
703 (AEs) during the freezing exotherm measured at the stem base (C) for four saturated samples

(water potential, Ψ, between −0.3 MPa and −0.5 MPa), three dry samples (Ψ between −3.2 MPa and −3.4 MPa) and three very dry samples (Ψ lower than −4 MPa). Significant differences ($P < 0.05$) between groups are indicated by different letters. Mean ± standard error.

Figure 7. Time series of CO_2 efflux and acoustic emissions (AEs; see also Fig. 1) from a *Picea abies* sample during three subsequent frost cycles. At the beginning of the experiment, sample water potential was −0.8 MPa. The background color represents the frozen (white) and thawed (light gray) periods of the xylem sap, white arrows show freezing-related CO_2 bursts, and gray arrows show thawing-induced CO_2 bursts.

Figure 8. Time series of CO_2 efflux and modeled respiratory CO_2 release (A) and cumulative number of acoustic emissions (AEs) (B) from a *Salix caprea* sample. At the beginning of the experiment, sample water potential was −0.3 MPa. Xylem temperatures inside the cuvette is shown in A (T2 and T3), whereas xylem temperature outside the cuvette in sample base (T1) and top (T4) is shown in B. The background color represents the frozen (white) and thawed (light gray) periods of the xylem sap.

Figure 9. Schematic of freezing in xylem and underlying processes of gas bursts and acoustic emissions (AEs) during ice propagation. The schematic is presented separately for a saturated (A), dry (B) and a very dry branch (C).

729 **Figures**

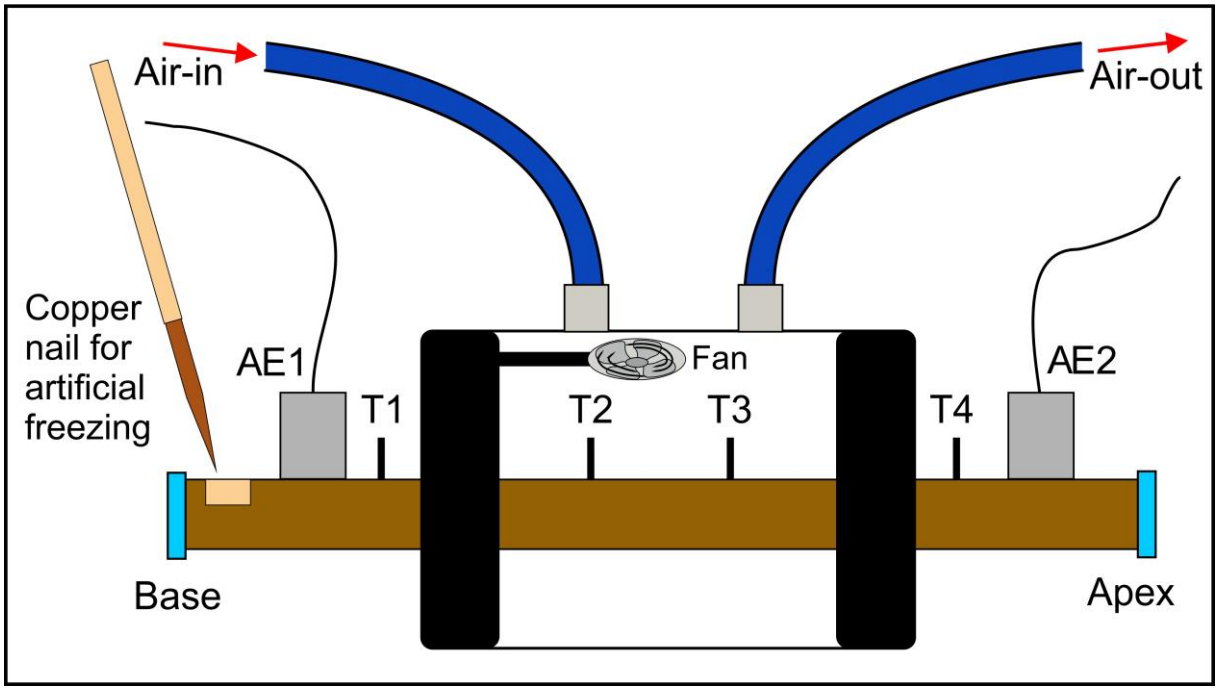

730

731 **Fig. 1**

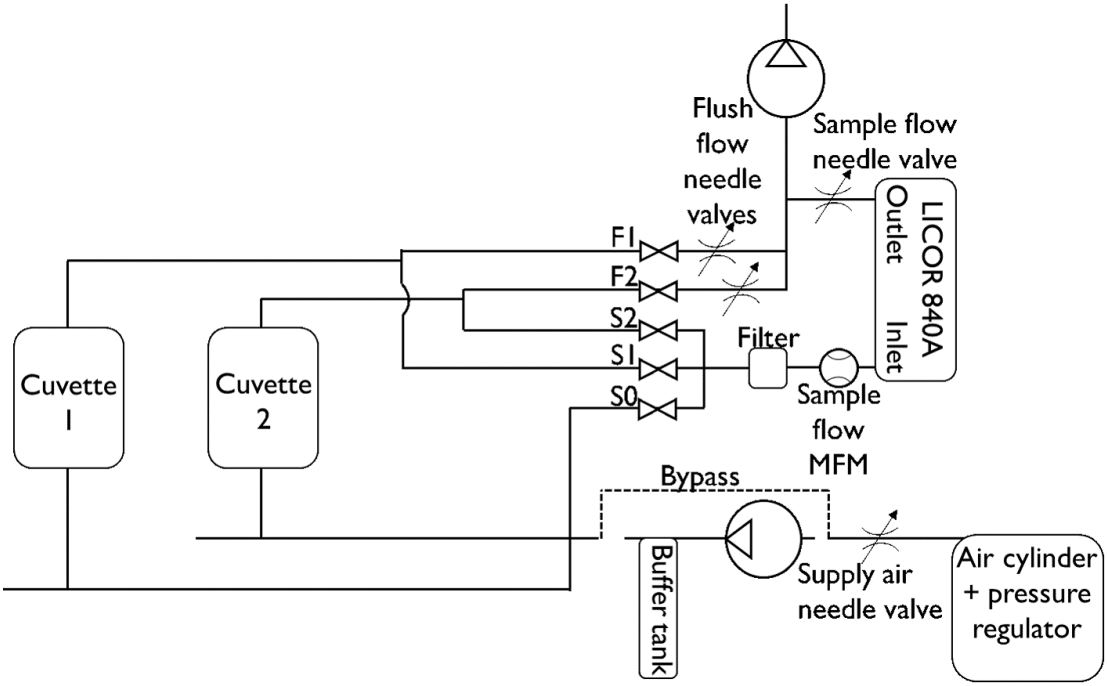

732

733 **Fig. 2**

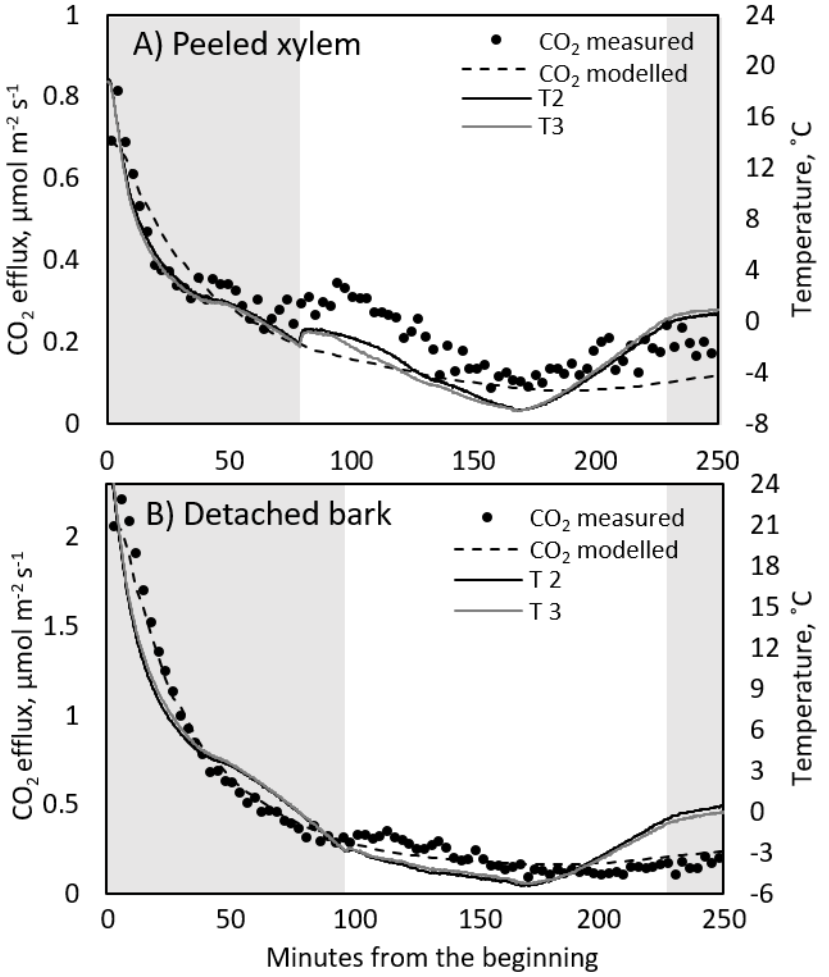
A) Peeled xylem
CO2 measured
CO2 modelled
T2
T3
CO2 efflux, µmol m-2 s-1
Temperature, ˚C
B) Detached bark
CO2 measured
CO2 modelled
T 2
T 3
CO2 efflux, µmol m-2 s-1
Temperature, ˚C
Minutes from the beginning

734

735 **Fig. 3**

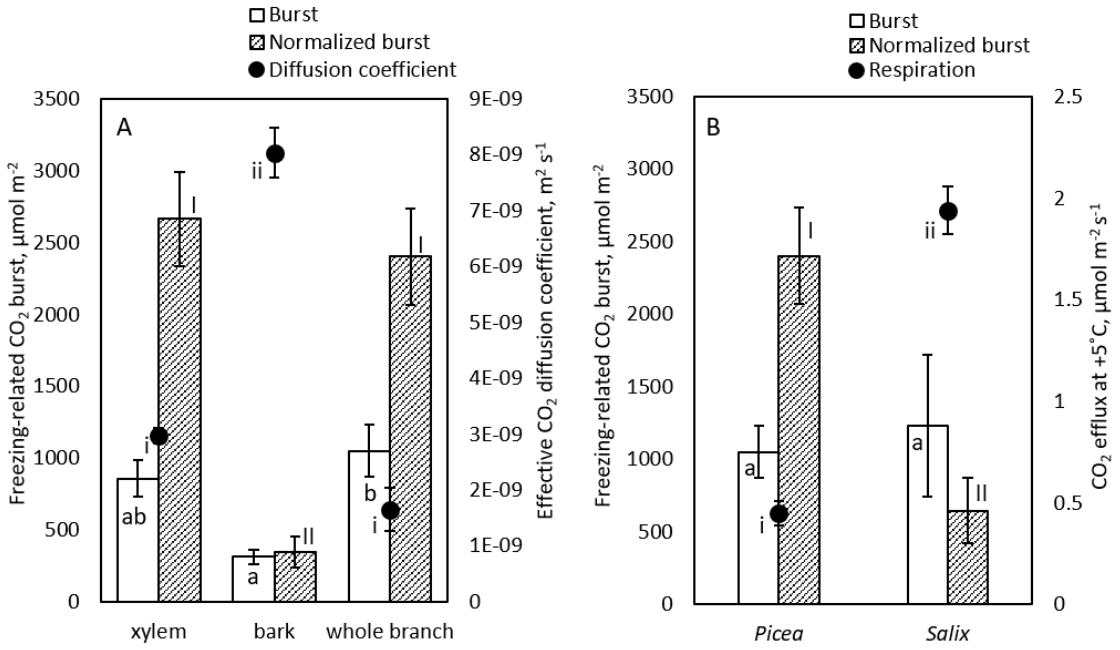
Burst
Normalized burst
Diffusion coefficient
A
Freezing-related CO_2 burst, µmol m^{-2}
Effective CO_2 diffusion coefficient, m^2 s^{-1}
3500
3000
2500
2000
1500
1000
500
0
9E-09
8E-09
7E-09
6E-09
5E-09
4E-09
3E-09
2E-09
1E-09
0
ab
a
b
i
ii
i
I
II
I
xylem
bark
whole branch
Burst
Normalized burst
Respiration
B
Freezing-related CO_2 burst, µmol m^{-2}
CO_2 efflux at +5°C, µmol m^{-2} s^{-1}
2.5
2
1.5
1
0.5
0
a
i
I
ii
II
Picea
Salix

736

737 **Fig. 4**

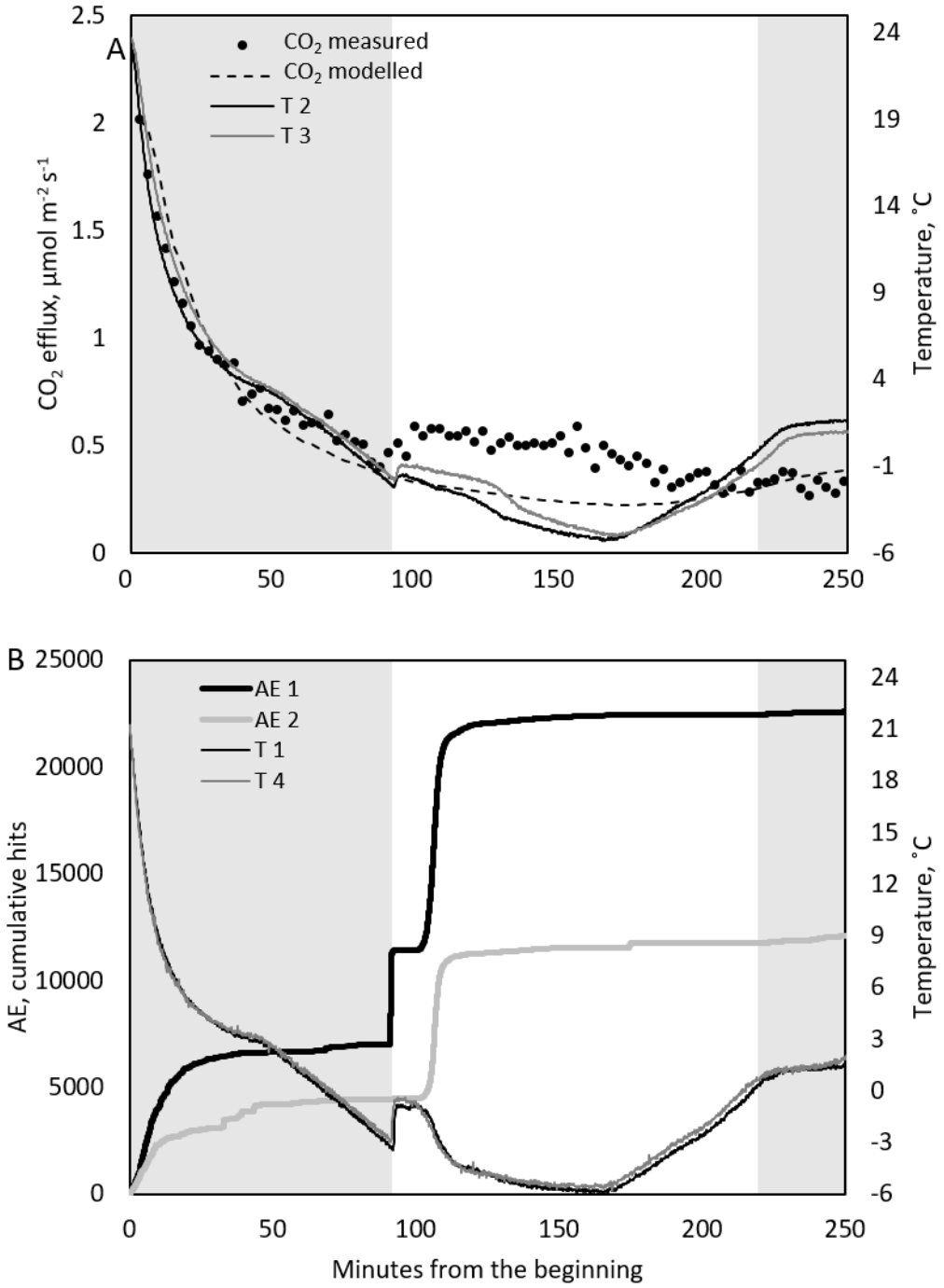
A
CO_2 measured
CO_2 modelled
T 2
T 3
CO_2 efflux, µmol m^{-2} s^{-1}
Temperature, °C
B
AE 1
AE 2
T 1
T 4
AE, cumulative hits
Temperature, °C
Minutes from the beginning

738

739 **Fig. 5**

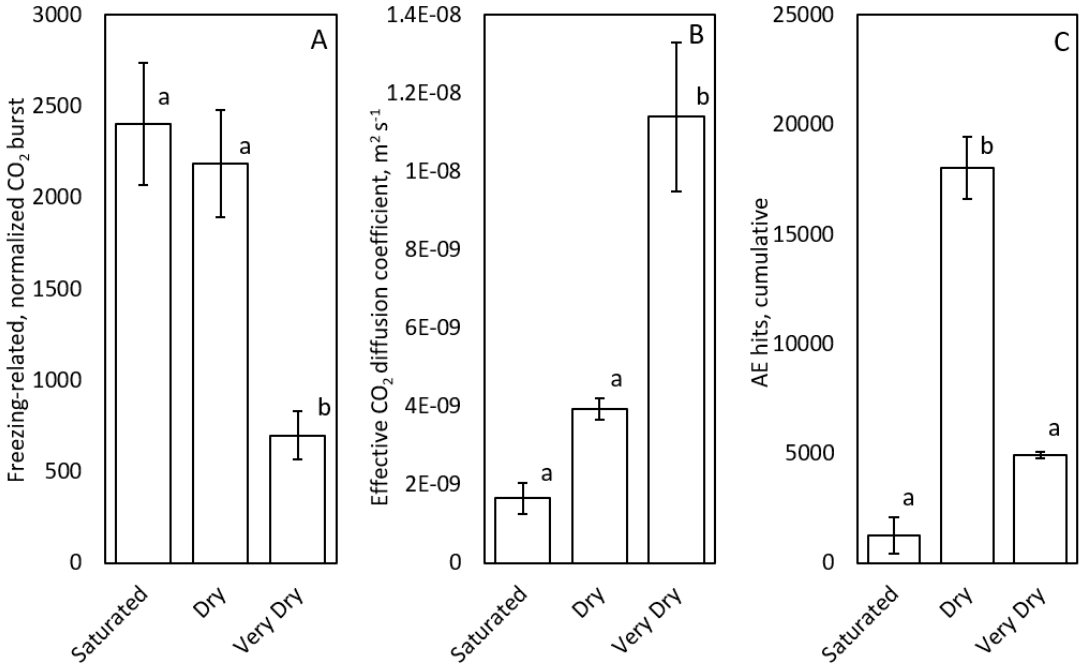

740

741 **Fig. 6**

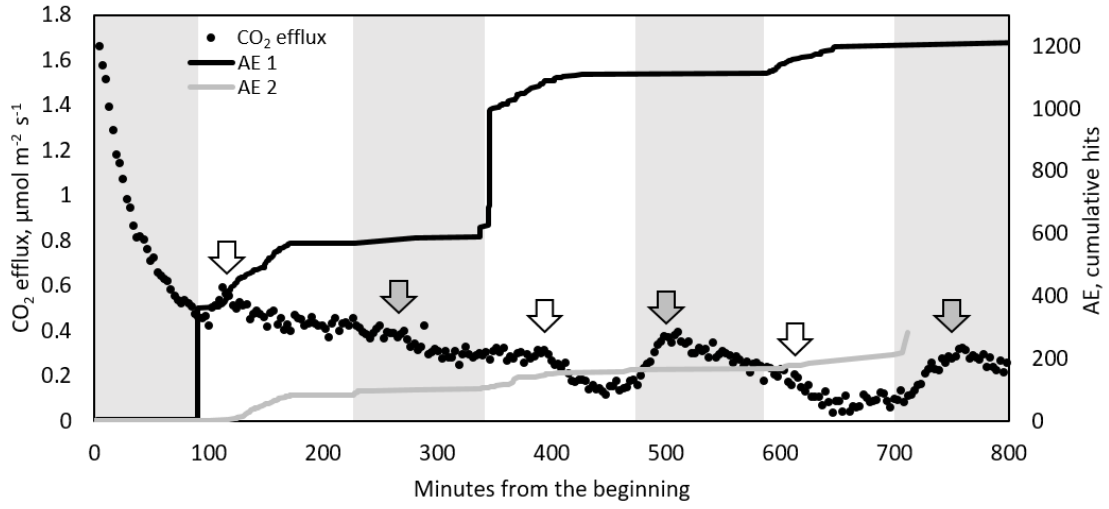

742

743 **Fig. 7**

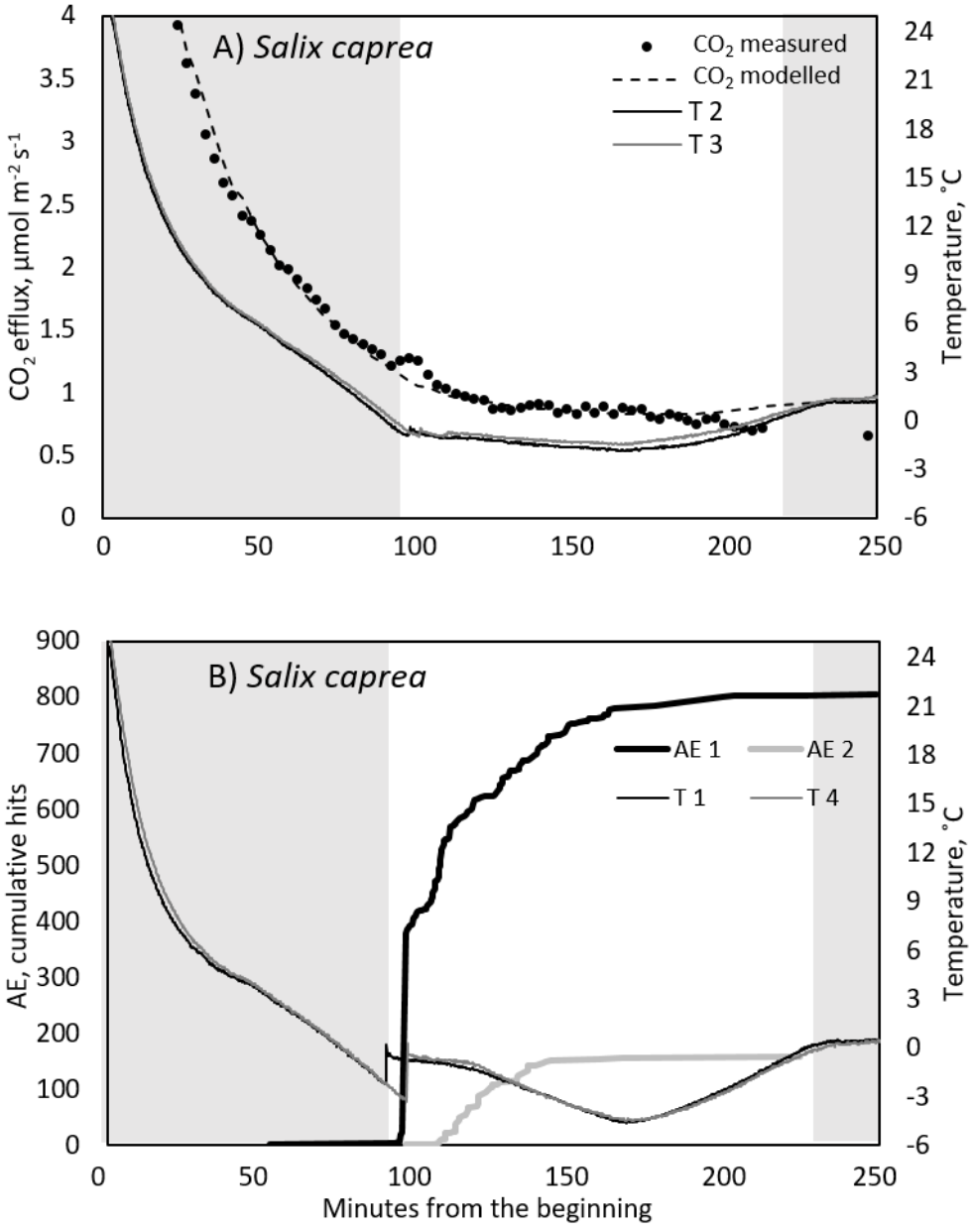
A) Salix caprea
CO2 measured
CO2 modelled
T 2
T 3
CO2 efflux, µmol m-2 s-1
Temperature, °C
B) Salix caprea
AE 1
AE 2
T 1
T 4
AE, cumulative hits
Minutes from the beginning

744

745 **Fig. 8**

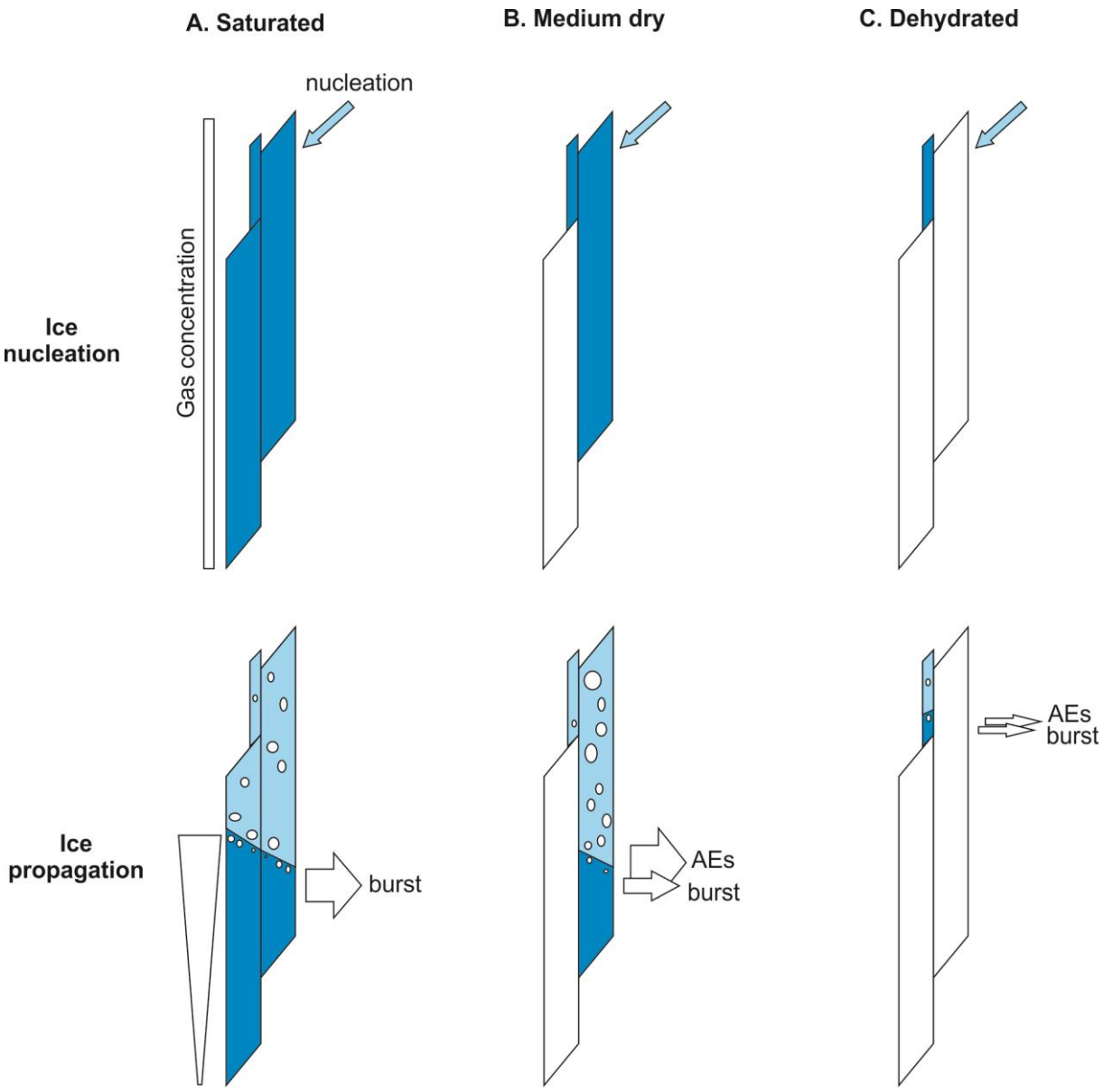

746

747 **Fig. 9**

748